



This is a repository copy of *Glue-laminated bamboo for dowel-type moment-resisting connections*.

White Rose Research Online URL for this paper:
<https://eprints.whiterose.ac.uk/172700/>

Version: Accepted Version

Article:

Wang, T.-H., Chung, Y.-L., Wang, S.-Y. et al. (1 more author) (2021) Glue-laminated bamboo for dowel-type moment-resisting connections. *Composite Structures*, 267. 113848. ISSN 0263-8223

<https://doi.org/10.1016/j.compstruct.2021.113848>

Article available under the terms of the CC-BY-NC-ND licence
(<https://creativecommons.org/licenses/by-nc-nd/4.0/>).

Reuse

This article is distributed under the terms of the Creative Commons Attribution-NonCommercial-NoDerivs (CC BY-NC-ND) licence. This licence only allows you to download this work and share it with others as long as you credit the authors, but you can't change the article in any way or use it commercially. More information and the full terms of the licence here: <https://creativecommons.org/licenses/>

Takedown

If you consider content in White Rose Research Online to be in breach of UK law, please notify us by emailing eprints@whiterose.ac.uk including the URL of the record and the reason for the withdrawal request.



eprints@whiterose.ac.uk
<https://eprints.whiterose.ac.uk/>

Glue-laminated bamboo for dowel-type moment-resisting connections

Tsung-Hsien Wang^{a*}; Yu-Lin Chung^b; Shih-Yuan Wang^c; Wen-Shao Chang^a

^a School of Architecture, University of Sheffield

Western Bank, Sheffield S10 2TN, UK

^b Department of Architecture, National Cheng Kung University

1 University Road, Tainan City, 701, Taiwan

^c Graduate Institute of Architecture, National Chiao Tung University

1001 University Road, Hsinchu, 300, Taiwan

* Corresponding Author

Tsung-Hsien Wang

Email: tsung-hsien.wang@sheffield.ac.uk

Phone: +44 (0)754 371 5664

Abstract

Research efforts have been devoted to glue-laminated bamboo (GLB) as an alternative to engineered timber. However, some research has shown that GLB exhibits brittle failure at smaller displacement when compared with Glulam. To address this issue and enhance the GLB mechanical performance, we propose to use Glass Fibre Reinforced Polymer (GFRP) to reinforce the GLB in the moment-resisting connections. A total of 24 GLB connections were tested to discuss the effectiveness of different reinforcement strategies. The test results showed that the connections reinforced by GFRP on both sides underwent significantly higher deformation before reaching the ultimate strength, which demonstrates the enhanced deformability of the connections. The ultimate moment-resisting strength could increase up to 37% compared to the unreinforced ones. Push-over analyses were carried out in this study to understand the effectiveness of different reinforcement strategies on the connections in portal frames, and this justifies the use of double-sided GFRP reinforcement.

Keywords

glue-laminated bamboo; dowel-type connection; moment-resisting strength; glass fibre reinforced polymer.

1. Introduction

With a growing interest in low carbon materials to mitigate greenhouse emissions, bamboo is gaining popularity as an emerging renewable building material for construction (Chung and Yu 2002; Trujillo et al. 2013). Due to its irregular geometrical appearance, processing bamboo culms into laminated composites is preferred. Laminating bamboo strips provides a standardised approach of tackling the challenges in natural material variations and makes laminated bamboo composites suitable for large scale industrial uptake. Recent studies (Sharma et al. 2017; Huang et al. 2019) showed that laminated bamboo composites have comparable mechanical properties as conventional timber-based products and the potential to be used in large scale structure design and construction. In addition to the well-known lightweight fibrous property of bamboo, advantages, including low thermal conductivity, high strength-to-weight ratio, fast-growing rate, and low cost, make this emerging material competitive with prevailing timber-based products (Ramirez et al. 2012; Shah et al. 2016). Albeit laminated bamboo composites are commercially available, the successful use of bamboo as a building material still requires a comprehensive understanding of its mechanical properties and the applicable joint mechanism in the larger scale structural application (Trujillo and Wang 2015; Wang et al. 2017).

Recent studies showed that the mechanical properties of engineering bamboo products are under the predominant influence of chosen processing methods, such as the chemical treatment of bleaching or caramelisation for preservation (Sharma et al. 2015b, 2018; Shah et al. 2018). In particular, the thermal treatment could significantly affect the mechanical properties of laminated bamboo products in bending with about 20% increase in compressive and shear strength parallel-to-the-grain. However, the thermal treatment would also create a more brittle material with the common failure mode of longitudinal splitting (Sharma et al. 2015b; Reynolds et al. 2019). The bending stiffness is correlated with the bamboo strip density, where the smaller strips leading to the higher fibre volume fraction could increase the bending stiffness (Penellum et al. 2018). Another factor—growth portion height, which varies from the growing portions of bamboo culms—exhibits a clear impact on the compressive strength (Li et al. 2013). Albeit these characterised strengths in the laminated bamboo composite provide great potential for construction, standardising manufacture processes and codifying the structural use of this emerging material would still be required to accelerate the adoption in the building and construction sector (Gat6o et al. 2014).

Studies on employing timber standards for characterisation showed that glue-laminated bamboo (GLB) products have properties comparable, and, in some areas, superior to timber-based products (Sharma et al. 2015a). While considering GLB for structural elements—such as beams, bending directions and internal joint locations would influence the mechanical properties; specifically, the latter—the internal joint location—could have more impact on the tangential bending (Li et al. 2018). A few studies on dowel-type connections were carried out to investigate the stress distribution at the connections with associated fracture behaviours in GLB. The embedment strength in the parallel-to-the-grain direction is higher than that in the perpendicular-to-the-grain direction and closely related to underlying parameters such as the number, dimensions, locations of the dowels, and the spacing between them (Ramirez et al. 2012; Sharma et al. 2017; Tang et al. 2019). The predominant failure mode observed was the brittle splitting along the longitudinal fibre direction. Further studies showed that common failures in the GLB dowel connections occurred mainly due to shear parallel to the grain and tensile perpendicular to the grain in the connection area (Lathuillière et al. 2015; Reynolds et al. 2016). To test the effective use of GLB in construction, limited efforts have been placed to investigate the dowel type GLB connections subjected to bending moment (Zhou et al. 2018; Leng et al. 2020), and the brittle failure parallel to the grain from the connection was observed.

Previous studies on improving the moment capacity of the dowel type timber connections suggested that applying reinforcement materials, such as steel plates (Metelli et al. 2016), fibre-reinforced polymers (FRP) (Schober and Rautenstrauch 2007; Alhayek and Svecova 2012), and self-tapping screws (Lathuillière et al. 2015; Zhang et al. 2019), could increase the ductility and mitigate the brittle failure with satisfactory effect. Albeit GLB is believed to be a good alternative solution to timber-based products, such as Cross-laminated timber (CLT), its reinforcement strategies, especially to their failure mechanisms, remain unexplored.

The embedment strength is an essential characteristic to establish a comprehensive understanding of GLB. Nevertheless, more efforts are still required to investigate the applications of GLB dowel-type connections subjected to bending moment. This paper, therefore, aims to fill in this knowledge gap and, at the same time, investigates a new strategy to reinforce this type of connection with GLB. Previous studies in timber beams showed that the flexural strength could be increased significantly when reinforcing with FRP (De La Rosa

García et al. 2013; Yang et al. 2013; Gómez et al. 2019). Applicable reinforcement strategies include the use of bars and laminates with glass, basalt, or carbon fibres (Li et al. 2014; Titirla et al. 2019; Shekarchi et al. 2020). The implementation was carried out through either inserting inside the structural elements, or, attaching directly onto targeted surface areas (Triantafillou 1997; Morales-Conde et al. 2015; Titirla et al. 2019). A significant increase of up to 183% could be achieved, as demonstrated by Kim and Harries (Kim and Harries 2010). Despite the prevalent use of carbon FRP, Gómez et al. found the basalt and glass fibres, even with a lower elastic modulus, exhibited superior results in increasing both the bending strength and ductility (Gómez et al. 2019).

To contribute the knowledge gap in dowel type GLB connections and its practical reinforcement strategies, Glass Fibre Reinforced Polymer (GFRP) is chosen because of its higher average ductile capacity and its superior strength-to-weight ratio. The intention is to apply GFRP for reinforcing GLB dowel-type connections, where the brittle failure, i.e., longitudinal splitting along the grain, occurs. The advantage of the GFRP high tensile strength is envisaged to minimise the crack propagation along the grain in a connection caused by bending. As discussed in the previous study for timber columns (Chang 2015), the density of reinforcement material possesses a strong correlation with the load-carrying capacity and the axial stiffness. In this paper, a series of tests were planned and carried out with variable reinforcement surface ratios to investigate the effectiveness of employing GFRP to enhance the mechanical properties of GLB dowel-type connections under bending moment.

2. Materials and Methods

This study considers a single beam consisting of GLB members with a steel plate to simulate a bamboo-steel-bamboo connection, as shown in Fig. 1. The GLB member has a dimension of 900mm in length, 120mm in depth, and 40mm in thickness. A total of 24 dowel-type connections are tested and prepared into four test groups. The experiment design is to investigate the structural performance of the GLB dowel-type connections and the strength improvement from the Glass Fibre Reinforced Polymer (GFRP). The proposed specimen experiment and the dowel configuration were designed based on EuroCode 5 (BSI 2009). We envisage this same design principle to be applicable for future follow-up applications.

The test grouping is based on the application of GFRP using four different surface reinforcement ratios, 0%, 18%, 30%, and 60%, respectively. In this study, the surface

reinforcement ratio of GFRP is calculated by dividing the total GFRP reinforced surface area with the fastener group surface area on both sides of the specimens. The intention is to gauge the impacts of applying GFRP reinforcement in GLB moment-resisting connections. The fastener group surface area covers nine 8mm fasteners from the end of the specimen, as shown in Fig. 1(b), where the base surface area has a dimension of 260 mm in length and 120mm in width. These four test groups are (1) ORL, (2) S3FRP, (3) S5FRP, and (4) D5FRP. ORL represents the group members without any GFRP reinforcement (0%), S3FRP for the outer surface application with the level 1 GFRP reinforcement (18%), S5FRP for the outer surface application with the level 2 GFRP reinforcement (30%), and D5FRP for the outer and inner surface application with the level 3 GFRP reinforcement (60%). As shown in Fig. 1(b), the associated GFRP locations are shaded in green for three reinforced groups, including S3FRP, S5FRP, and D5FRP. The GFRP reinforcement level is determined by the number of GFRP strips applied on the fastener group surface area.

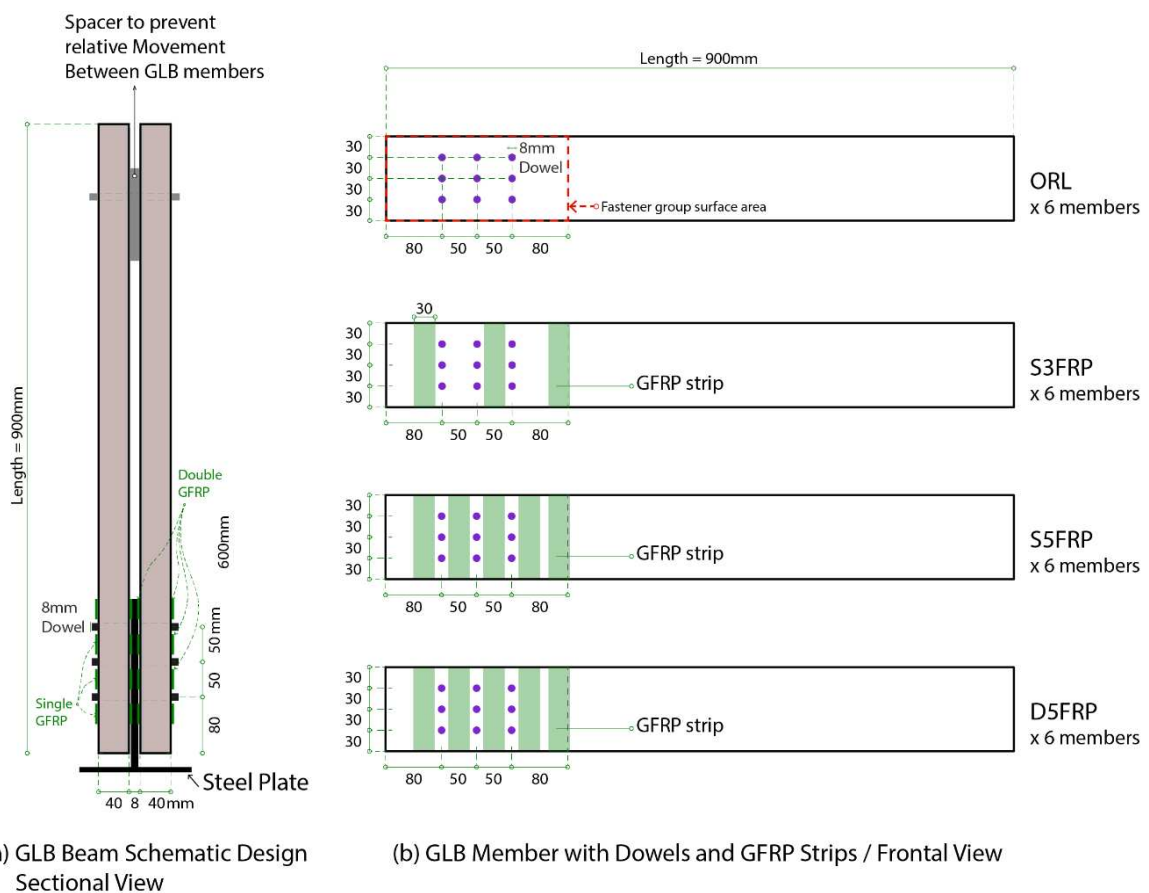


Fig. 1 Four specimens, ORL, S3FRP, S5FRP, D5FRP.

ORL: original laminated-bamboo specimen without GFRP reinforcement; S3FRP: 18% GFRP reinforcement on one side of the specimen; S5FRP: 30% GFRP reinforced specimen (Single-sided); D5FRP: 60% GFRP reinforced specimen (Double-sided)

2.1 Glue-Laminated Bamboo (GLB) Fabrication

Glue-laminated bamboo specimens were manufactured from *Phyllostachys edulis*—Moso bamboo—acquired in Taiwan with a resorcinol resin. The average diameter of a Moso bamboo culm is between 14 and 15 centimetres. The process of manufacturing the laminated bamboo (Fig. 2) includes five major steps: (1) splitting bamboo culms into strips, (2) preserving bamboo strips by NaOH solution, (3) drying bamboo strips to around 15% moisture content, (4) planing bamboo strips to 6mm in thickness, and (5) gluing and pressing bamboo strips. The initial bamboo culms were first split into strips with 40mm in width and then boiled in NaOH solution. During the drying process, bamboo strips were kept in the controlled chamber with a temperature between 45 to 50 Celsius and 20% relative humidity for consecutive 72 hours before post-processing the thickness for the final lamination. The resorcinol resin adhesive was applied with a glue proportion of approximately 1250g per square meters. The manual clamps were utilised with the required pressure of a minimum of 0.6 MPa for a minimum of 12 hours.



Fig. 2 The manufacturing process of glue-laminated bamboo in Taiwan

2.2 Doweled GLB Connection

The bamboo-steel-bamboo connections consisted of 8mm steel plates assembled with two GLB members that have 40mm in thickness. The configuration of connections was designed according to Eurocode 5 (EC5 hereafter) (BSI 2009). The dowel's diameter was 8 millimetres, and a three-by-three fastener group was employed for the bamboo-steel-bamboo connection studied in this paper. The steel dowels and plates were made from the steel with the tensile strength of 400 to 510 MPa. Nine-millimetre holes were prepared with GLB specimens for the bamboo-steel-bamboo dowel-type connection.

In this study, Durostone® UTR was chosen for the reinforcement. The GFRP strips of 30 mm in width by 120 mm in length were prepared and later glued onto the specimen surface using a variable surface reinforcement ratio. The mechanical properties of chosen GFRP are shown in Table 1, where the modulus of elasticity, E_f , is 11700 MPa for 0.8mm thick GFRP. The unit axial stiffness per unit width (E_{ff}) is therefore 9.36 GPa. In Table 1, perpendicular and parallel refer to the loading directions of the laminates/sheet when tested.

Table 1 Mechanical properties of Durostone® UTR

| GFRP Product | Format size L x W (mm) | Thickness (mm) | Mechanical properties | | | |
|--------------------|---------------------------|-------------------|--|--|---|--------------------------------------|
| | | | Bending strength (perpendicular) (MPa) | Modulus of elasticity (perpendicular) (MPa) | Compressive strength (perpendicular) (MPa) | Tensile strength (parallel) (MPa) |
| Durostone - UTR | 1828 x 914 | 0.8 | 152 | 11700 | 228 | 54 |

For high strength structural bonds, we use the industrial-grade epoxy adhesive, Hysol E-60hp, suitable for bonding wood and plastic products. The fully cured epoxy has a tensile strength of 35.2 MPa and a shear strength of 11.3 MPa for wood products. For each GFRP strip, the entire contact surface was coated with epoxy adhesive to join GLB members with contact pressure for consecutive 24 hours to reach its full bonding strength before tests. The designated GFRP locations for the reinforcement are illustrated in Fig. 1 above.

2.3 Digital Image Correlation for Strain Field Visualisation

Before the moment tests, selected specimens were painted with black speckle patterns in a matt white background for Digital Image Correlation (DIC). The painted pattern covered a surface area of 120mm x 260mm, where the nine fasteners were located. The objective of

using DIC was to monitor the full-field crack propagation and observe the strain distribution with and without GFRP reinforcement. The painted pattern (as shown in Fig. 3) has no physical effect on the specimen and, as such, no anticipated difference in the cracks occurring during the tests.

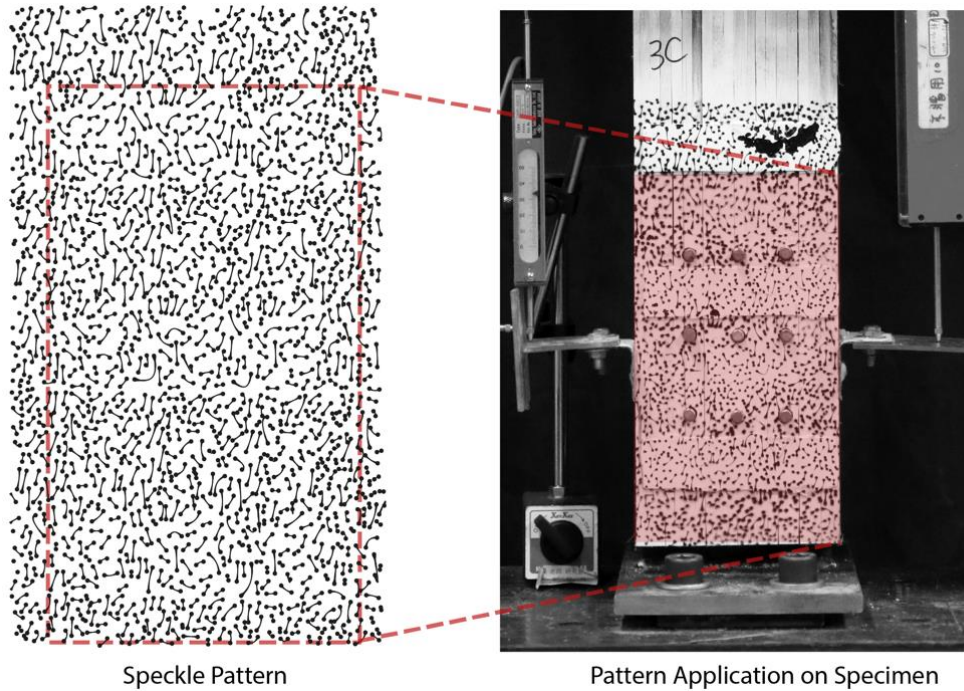


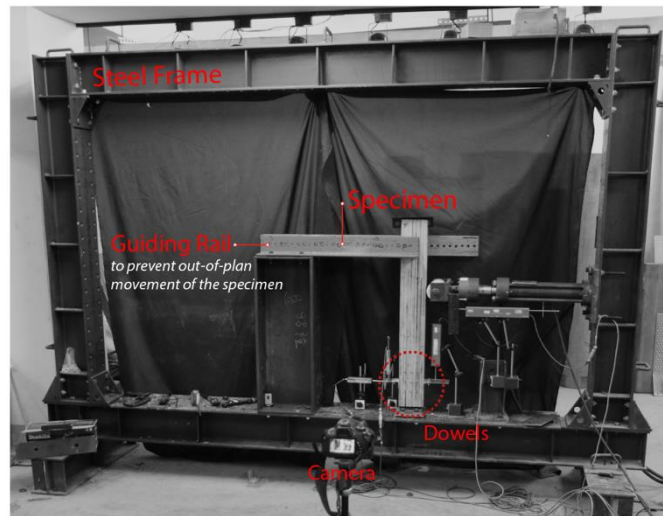
Fig. 3 (Left) The Speckle pattern designed for Digital Image Correlation; (Right) The specimen with the pattern applied on a matte white finish.

2.4 GLB Moment Connection Test Set-up

For the moment-resisting test, the GLB beam and the connecting steel plate were placed within the steel frame (Fig. 4). The GLB beam was anchored on the base of the steel frame, and a ten metric ton hydraulic jack was bolted horizontally to the steel frame for monotonic loading. The hydraulic jack pushed the GLB beam horizontally at a distance of 600mm from the end of the GLB beam at the bottom. Steel blocks were employed as the guiding rail to prevent the specimen's out-of-plane movement during the test. Continuous loading was terminated when the connection capacity dropped to less than 85% of the observed maximum capacity. Loading was applied at a speed of 0.1 mm per second and digital images were taken at a 30-seconds interval for the DIC analysis.

Fig. 4 illustrates the moment-resisting test set-up, and a total of four linear variable differential transformer (LVDT) were deployed. LVDT01 and LVDT04 measured the

horizontal displacement at the loading point and the centre of the fastener group respectively. LVDT 02 and LVDT03 measured the vertical movement along with the centre fastener group.



(a) Experiment Set Up

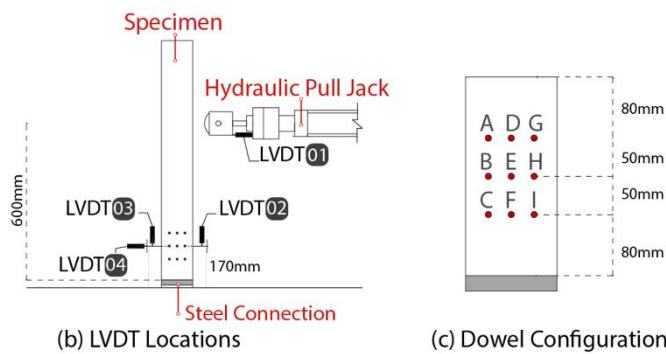


Fig. 4 (a) Moment-resisting test set up; (b) Four linear variable differential transformer (LVDT) locations; (c) Dowel configuration at the connection

3. Results and Discussion

3.1 Moment-Rotation Relationship

In Table 2, we summarise the moment-resisting tests for four dowel-type connection groups—ORL, S3FRP, S5FRP and D5FRP. These test result values include: (1) the maximum moment capacity in kNm; (2) the maximum displacement at maximum capacity in mm; (3) the moment capacity at first failure occurred in kNm; (4) the displacement at first failure occurred in mm, and (5) crack occurrence, which records cracks observed with specific dowel locations per specimen. The experiment data are collected to examine the correlation between the strength improvement with their associated displacements and the applications

of GFRP with varied reinforced surface ratios. The expected findings are to understand the applicability of GFRP reinforcement in GLB connections.

Table 2 The summary of the moment-resisting test results for all groups

| Specimen ID | Max Moment Capacity (kNm) | Disp. @ Peak (mm) | Moment Capacity @ 1st Failure (kNm) | Disp. @ 1st Failure (mm) | Crack Occurrence @ Dowel Location |
|-------------|---------------------------|-------------------|-------------------------------------|--------------------------|--|
| ORL01 | 2.745 | 36.835 | 2.666 | 37.279 | Cracks at Front[A,B,G,H,I] |
| ORL02 | 3.128 | 50.746 | 3.028 | 41.012 | Cracks at Front[A,B] |
| ORL03 | 2.357 | 33.022 | 2.295 | 33.237 | Cracks at Front[B,C,G,H,I] |
| ORL04 | 2.242 | 56.418 | 1.838 | 20.249 | Cracks at Rear[A,B,C,H,I] |
| ORL05 | 2.365 | 49.052 | 2.045 | 34.201 | Cracks at Front[A,B,C, G,H,I] Rear[A,B,C] |
| ORL06 | 2.528 | 41.804 | 2.215 | 29.150 | Cracks at Front[G,H,I] Rear[D,E,F,G,H] |
| S3FRP01 | 2.803 | 38.679 | 2.707 | 38.798 | Cracks at Rear[A,B,C,G,H,I] |
| S3FRP02 | 2.206 | 30.197 | 2.130 | 31.399 | Cracks at Front[A,B, H,I] Rear[A,B] |
| S3FRP03 | 2.893 | 42.836 | 2.788 | 43.609 | Cracks at Front[A,B,C,I] Rear[A,B,C,G,H] |
| S3FRP04 | 2.893 | 51.924 | 2.419 | 36.387 | Cracks at Front[A,B,H,I] Rear[B,C,D,E,G,H,I] |
| S3FRP05 | 2.823 | 48.077 | 2.388 | 32.693 | Cracks at Front[A,B,C,G,H,I] Rear[A,B,C] |
| S3FRP06 | 2.779 | 41.142 | 2.588 | 30.221 | Cracks at Front[G,H,I] Rear[D,E,F,G,H] |
| S5FRP01 | 3.110 | 46.190 | 2.897 | 40.925 | Cracks at Rear[A,B,C,G,H,I] |
| S5FRP02 | 3.004 | 52.583 | 2.988 | 53.001 | Cracks at Rear[A,B,C,G,H,I] |
| S5FRP03 | 2.756 | 40.261 | 2.582 | 29.488 | Cracks at Rear[A,B,C] |
| S5FRP04 | 3.081 | 54.680 | 3.041 | 55.113 | Cracks at Front[A,B,G,H,I] |
| S5FRP05 | 2.812 | 38.997 | 2.741 | 39.343 | Cracks at Front[G,H,I] Rear[A,B,C,G,H] |
| S5FRP06 | 3.110 | 59.777 | 3.009 | 66.606 | Cracks at Rear[A,B,C] |
| D5FRP01 | 3.882 | 103.861 | 3.727 | 105.333 | Cracks at Front[A,B,C,G,H,I] Rear[B,C,G,H,I] |
| D5FRP02 | 3.539 | 66.850 | 3.46 | 68.574 | Cracks at Front[A,B,G,H,I] |
| D5FRP03 | 4.856 | 46.563 | 4.738 | 47.592 | Cracks at Front[A,B,G,H,I] Rear[A,B,C,D,E,F] |
| D5FRP04 | 3.372 | 48.120 | 3.265 | 48.852 | Cracks at Front[G,H,I] No cracks at Rear |
| D5FRP05 | 3.599 | 72.845 | 3.349 | 81.073 | Cracks at Front[A,B,E,H,I] |
| D5FRP06 | 3.176 | 54.645 | 3.071 | 55.162 | Cracks at Front[H,I] Rear[A,B,C,D,E] |

* Disp. values were the measured movement of the hydraulic pull jack by LVDT_01 as shown in Fig.4

These test results were further visualised in Fig. 5 for the moment-displacement relationships of four test groups. All groups display varied moment-displacement relationships due to local natural material defects, such as knots, yet the overall moment-displacement trends within each group were similar.

In Table 3, we summarise the results from the moment-resisting connection tests and show (1) Mean Ultimate Moment Capacity ($M_{ultimate}$), (2) Mean Displacement at Ultimate Moment Capacity ($Disp_{ultimate}$), (3) Mean Moment Capacity at First Failure (M_{crack}), and

(4) Mean Displacement at First Failure ($Disp_{crack}$). The coefficient of variance for each test group was also conducted to illustrate the extent of variability in each specimen group. The preliminary results show that the moment capacity increases when GFRP reinforcement is applied on either single or double sides of the specimen surfaces.

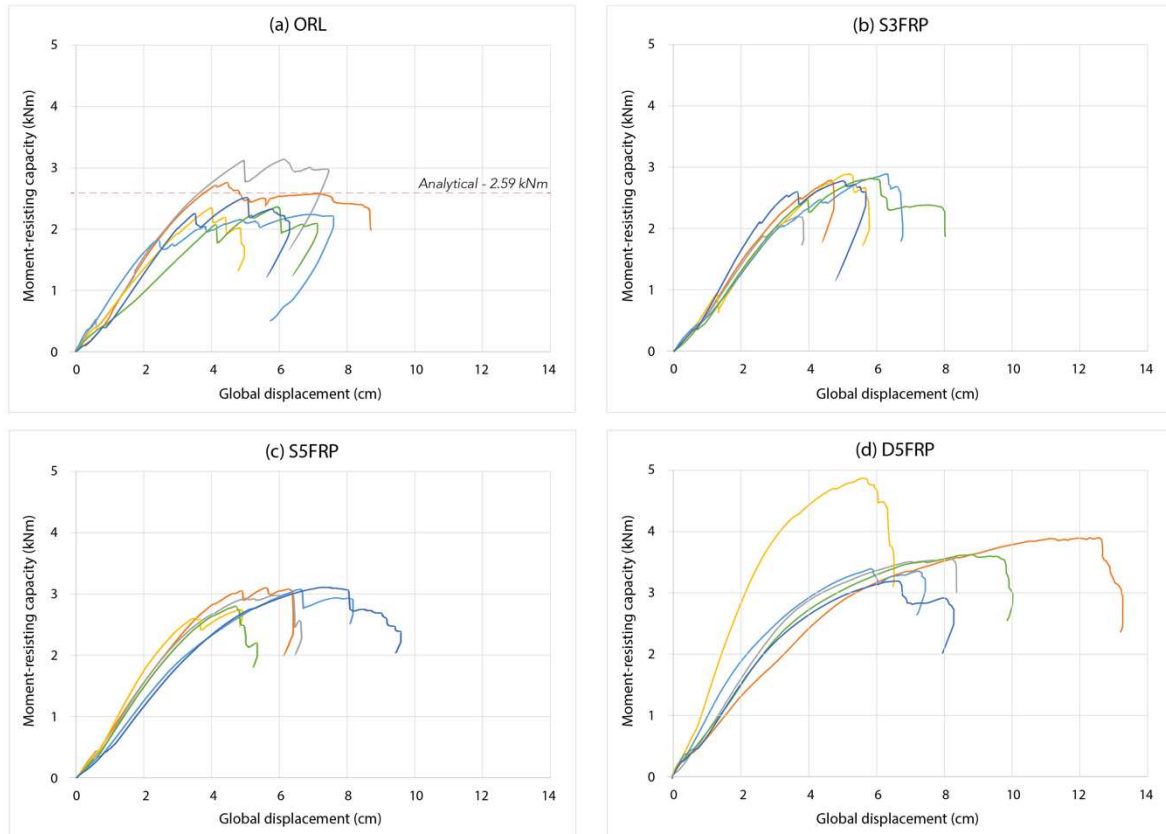


Fig. 5 Moment-resisting capacity with the global displacement for all test groups, (a) ORL, (b) S3FRP, (c) S5FRP and (d) D5FRP

Table 3 The summary of the test results for the mean moment capacity and displacement value with coefficient of variance

| Group ID | $M_{ultimate}^1$ (kNm) | $Disp_{ultimate}^2$ (%) | M_{crack}^3 (kNm) | $Disp_{crack}^4$ (%) |
|----------|------------------------|-------------------------|---------------------|----------------------|
| ORL | 2.56 (13%*) | 5.42 (20%) | 2.35 (18%) | 3.96 (22%) |
| S3FRP | 2.73 (10%) | 5.12 (18%) | 2.50 (10%) | 4.32 (14%) |
| S5FRP | 2.98 (5%) | 5.92 (17%) | 2.88 (6%) | 5.76 (28%) |
| D5FRP | 3.51 (7.5%) | 8.37 (31%) | 3.37 (7%) | 8.67(31%) |

¹ $M_{ultimate}$: Ultimate Moment Capacity

² $Disp_{ultimate}$: Displacement at Ultimate Moment Capacity

³ M_{crack} : Moment Capacity at First Failure

⁴ $Disp_{crack}$: Displacement at the first failure

* CoV – Coefficient of Variance

3.2 Effectiveness of the GFRP Reinforcement

In this section, we performed the univariate analysis of variance (ANOVA) tests and the pairwise comparisons to investigate the statistic difference among test groups for the ultimate moment capacity. Table 4 summarises the pairwise comparisons among four test groups using the dependent variable $M_{ultimate}$. The ANOVA tests and comparisons were conducted with six samples of ORL, S3FRP, and S5FRP groups and five samples of D5FRP, which excludes one outlier from the original dataset.

In the ultimate moment capacity test, there is a significant statistical difference between groups ($p = 0.000$), particularly when GFRP was applied on both sides of the specimen surfaces. The mean $M_{ultimate}$ of the D5FRP group is 37% higher as compared to the ORL group. Overall, the mean $M_{ultimate}$ of single-sided reinforcement groups shows a positive trend, where S3FRP is 6% higher than ORL, and S5FRP is 16% higher than ORL. To clarify the significant statistical difference between groups, we conduct the pairwise comparisons on the mean ultimate moment capacity for groups (Table 4). The D5FRP group exhibits a significant difference in $M_{ultimate}$ ($p < 0.05$) and illustrates a clear advantage in increasing moment-resisting capacity.

Table 4 The summary of ANOVA pairwise comparisons among test groups for $M_{ultimate}$

| | ORL | S3FRP | S5FRP | D5FRP |
|-------|---------------|---------------|---------------|-------|
| ORL | - | | | |
| S3FRP | 1.000 | - | | |
| S5FRP | 0.071 | 0.705 | - | |
| D5FRP | 0.000* | 0.001* | 0.018* | - |

* $p < 0.05$ indicates the mean difference between the two groups is statistically significant.

Albeit single-sided reinforcement groups, S3FRP and S5FRP, show higher mean $M_{ultimate}$ values as compared to the ORL group, the difference is not statistically significant ($p > 0.05$). When comparing test results of S3FRP to ORL groups, the GFRP configuration could not successfully stop crack propagation due to the low surface reinforcement ratio (18%). As such, S3FRP and ORL have no significant difference. When comparing S5FRP to ORL, the observed p-value of 0.071 indicates a narrow miss from the confidence level of 0.05. This comparison result may be caused by the small sample size of six per test group and the uncertainty in the crack occurrence on the side of the specimen surface without GFRP reinforcement. The observations and the pairwise comparisons support that applying GFRP reinforcement on both sides of specimen surfaces (D5FRP) could effectively stop crack

propagation ($p < 0.05$). Similarly, in the maximum displacement test, the pairwise comparisons show that the D5FRP group has a noticeable increase of 55% compared to the original unreinforced group—ORL ($p = 0.023$).

In brief, reinforcing the GLB beams using GFRP will delay the development of the first crack and, in turn, lead to larger displacements when the first crack is taking place. However, a significant difference only occurs in the D5FRP group. It indicates that double-sided GFRP reinforcement could improve the displacement and hence prolong the time to reach the first failure when the first crack occurs. This finding sustains that applying double-sided GFRP reinforcement will increase the ultimate moment capacity and enhance the connections' ductility.

3.3 Failure Modes

The dominant failure mode observed during the test was the splitting failure of the GLB beam parallel-to-the-grain. Cracks were mostly located at the top row of the first column and the bottom row of the last column of the fastener group, as shown in Fig. 6. The left image of Fig. 6 shows resulting cracks, and the right one visualises the in-situ full-field horizontal strain measurement overlaying the original specimen. All the observed splitting of laminated bamboo was sudden and accompanied by a significant load drop. In most cases, after the first failure occurred and before the ultimate moment capacity was reached, the maximum displacement continued increasing with the applied loads. As the cracks could happen on either side of the specimens, it was therefore limited when conducting a comprehensive observation using DIC, as DIC was only applied on one side of the specimen in the current test set-up.

When analysing the DIC results, a similar strain propagation pattern along the x-axis direction was observed. In Fig. 7, two DIC results for ORL06 and S3FRP05 were compared side by side. Both groups show a similar x-axis strain pattern—including vertical concentration aligned with the grain. The most significant strain occurred at the corners of the fastener group, particularly top-left and bottom-right corners.

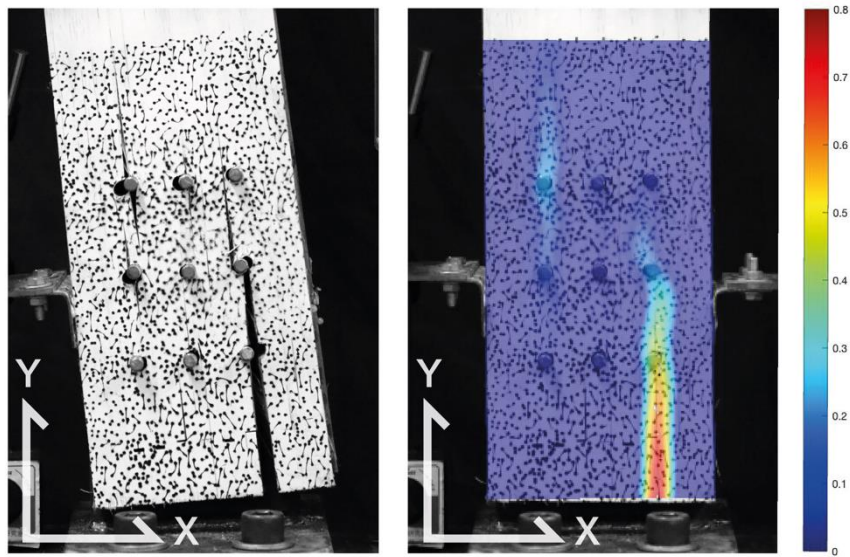


Fig. 6 Cracks shown at the top and middle rows of the first column and from the bottom row of the third column of the fastener group.
 (Left) ORL06 after failure detected; (Right) DIC analysis of the x-axis strain propagation

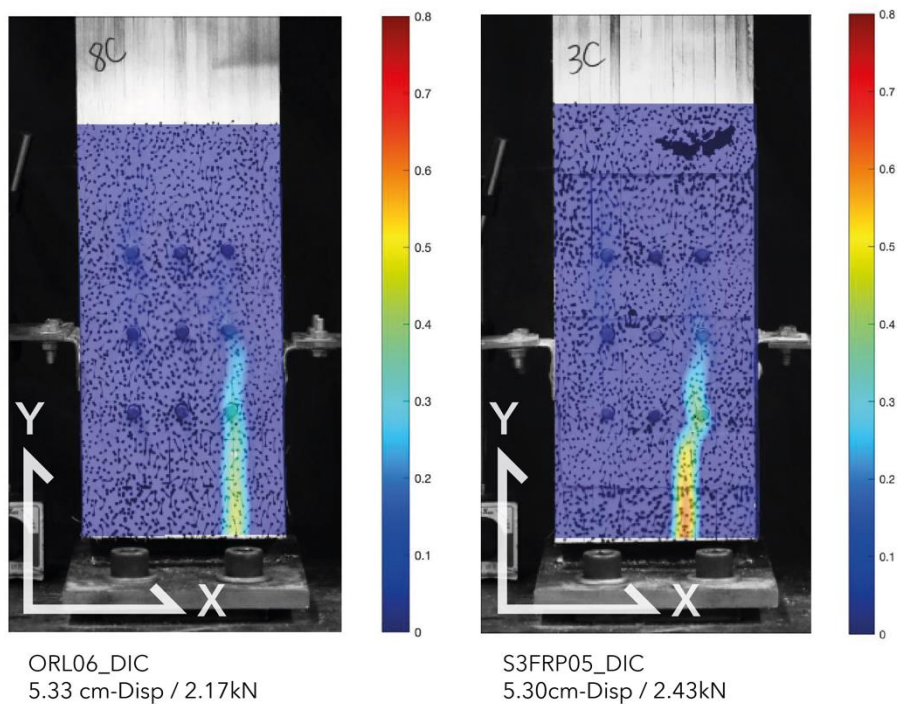


Fig. 7 DIC analysis results for ORL06 and S3FRP05

By comparing the occurrence of splitting failure along the grain for all test groups, a preliminary conclusion is that GFRP reinforcement will not reduce the chance of crack initiation nor change the locations of crack occurrence. However, GFRP reinforcement could prolong the time to develop the first crack and delay the propagation of the cracks with either

single- or double-sided reinforcement, leading to enhanced ductility of the connection. Previous research has concluded the failure mode of the GLB dowel-type connections being shear parallel to the grain (Reynolds et al. 2016), and this is different from our observation in the tests, which is tensile failure perpendicular to the grain. The main reason causing this difference is that the GLB beams were subject to bending moment in this study, whereas others were embedment tests with compression loading parallel to the grain.

From the geometry information, we noticed that dowels A, C, G and I have the largest lever arms, which implies these four dowels should have the largest displacement under the same rotation and in consequence these are where the most significant strain and stress concentration started as shown in Fig. 8. This explains the reason that the crack often occurred in these locations and then propagate to the adjacent dowels along the grain.

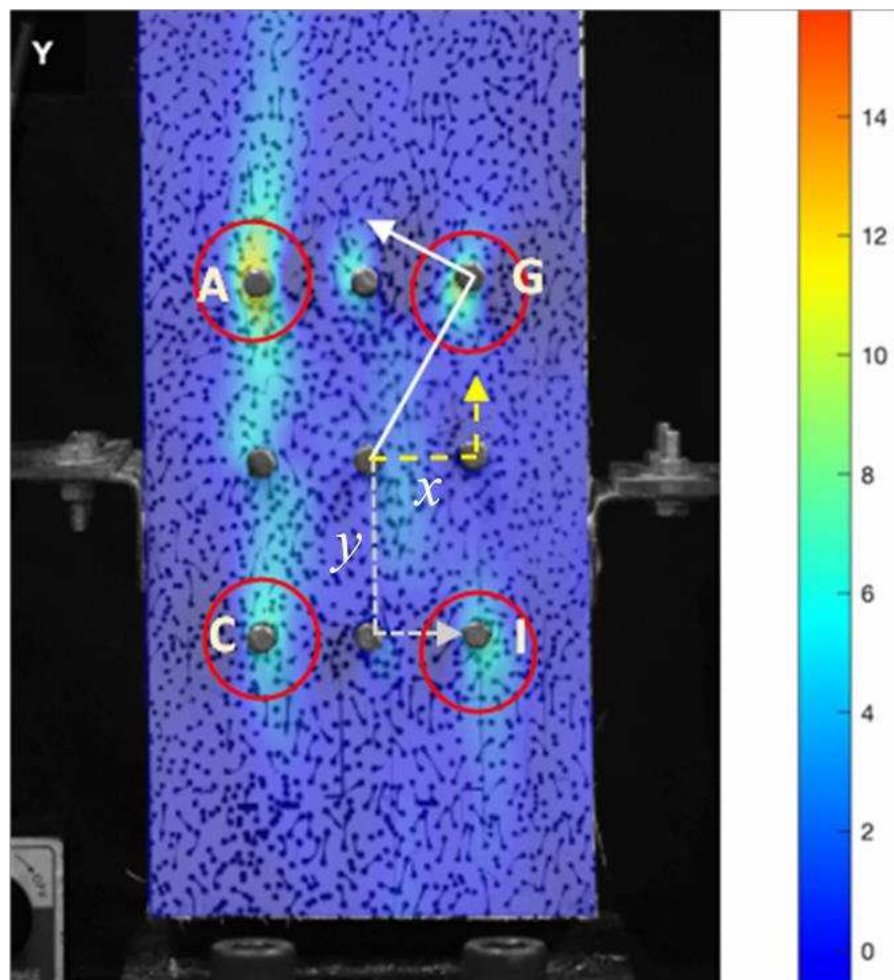


Fig. 8 The dowels A, C, G and I has the largest strain due to the longest lever arm

4 Estimation of moment capacity of unreinforced GLB connections

To estimate the moment capacity of the unreinforced GLB connections, it is essential to estimate the strength of each dowel. For the characteristic load-carrying, we assume the connection rotates about dowel E (Fig. 4c), as evidenced in the previous research by Zhang et al. (2019). The capacity of each dowel per shear plane can be calculated as (BSI 2009):

$$F_{v,Rk} = \min \left\{ \begin{array}{l} f_{h,1,k} t_1 d \\ f_{h,1,k} t_1 d \left[\sqrt{2 + \frac{4M_{y,Rk}}{f_{h,1,k} d t_1^2}} - 1 \right] \\ 2.3 \sqrt{M_{y,Rk} f_{h,1,k} d} \end{array} \right. \quad (1)$$

Where

$F_{v,Rk}$ is the characteristic load-carrying capacity of per steel dowel per shear plane

$f_{h,1,k}$ is the characteristic embedment strength of the side member

t_1 is the thickness of the side member

d is the diameter of the dowel

$M_{y,Rk}$ is the characteristic yield moment of the fastener

The characteristic yield moment of the fasteners can be calculated by:

$$M_{y,Rk} = 0.3 f_{u,k} d^{2.6} \quad (2)$$

Where $f_{u,k}$ is the ultimate tensile strength of the dowel (MPa)

The ultimate strength of the steel used in the dowel is 400 MPa, hence the characteristic yield moment of the fasteners can be calculated as:

$$M_{y,Rk} = 0.3 f_{u,k} d^{2.6} = 0.3 \times 400 \times 8^{2.6} = 26743 Nmm \quad (3)$$

In order to obtain the characteristic load-carrying capacity of each dowel, the embedment strength of each dowel was needed. Embedment tests were carried out to obtain the characteristic embedment strength of the GLB. According to BS EN 14358 (BSI 2016), experiments were carried out, and the experimental setup is illustrated in Fig. 9. Table 5 shows the experiment results.

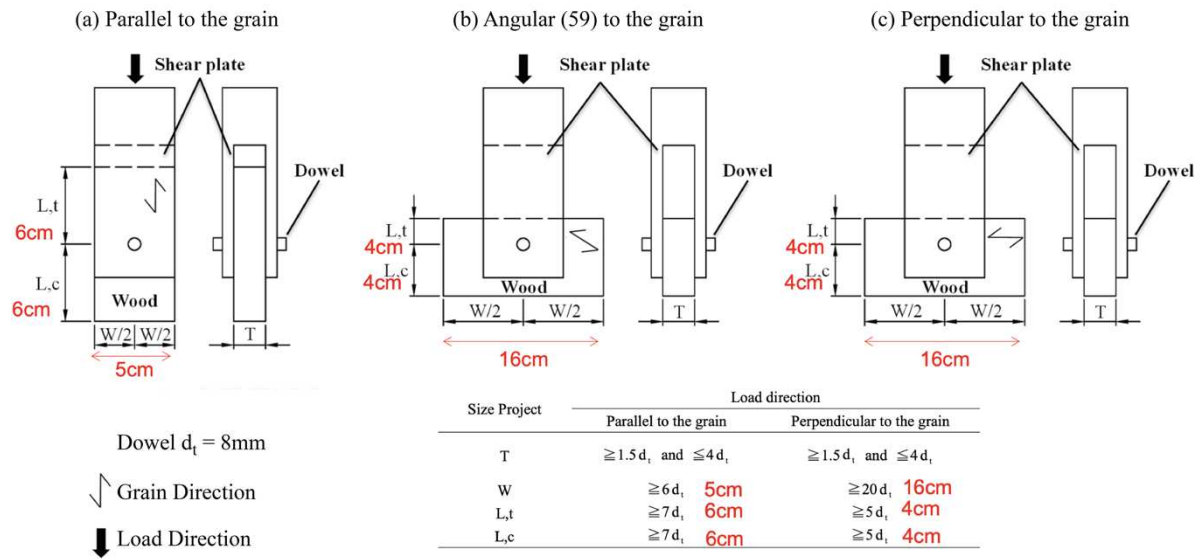


Fig. 9 The embedment experiment setup

Table 5 Results of embedment tests

| | No of specimens | Mean (MPa) | SD value | Characteristic value (MPa) |
|------------------|-----------------|------------|----------|----------------------------|
| $f_{h,k,0}$ * | 8 | 21.31 | 4.49 | 11.47 |
| $f_{h,k,90}$ ** | 7 | 12.14 | 3.27 | 4.99 |
| $f_{h,k,59}$ *** | 5 | 14.38 | 2.39 | 9.07 |

* Embedment strength of dowels B, H ;

** Embedment strength of dowels D, F;

*** Embedment strength of dowels A, C, G, I

By substituting the parameters in Table 5 and the characteristic yield moment of the fasteners into Equation (1), the Employing the parameters in Table 5, the characteristic load-carrying capacity of each dowel per shear plane can be tabulated as Table 6.

Table 6 The characteristic load-carrying capacity by Dowel

| | characteristic load-carrying capacity (N) | Dowel number |
|---------------|---|--------------|
| $F_{v,Rk,0}$ | 2392.6 | B, H |
| $F_{v,Rk,90}$ | 1386.8 | D, F |
| $F_{v,Rk,59}$ | 2058 | A, C, G, I |

The estimated characteristic moment capacity of the connection tested can be calculated by the following equation:

$$M_{RK} = F_{v,RK} \times \frac{\sum(x^2+y^2)}{r_{max}} \times n_{sp} \quad (4)$$

Where $F_{v,RK}$ is the characteristic load-carrying capacity of the dowels that control the failure of the connection, x is the spacing between dowels in horizontal direction (as shown in Fig.

1), y is the spacing between dowels in vertical direction, and r_{max} is the largest lever arm of the dowels as shown in Fig. 1, and n_{sp} is the number of the shear planes.

From Table 6, one can find that the characteristic moment capacity of the connection is limited by the dowel D and F, and hence $F_{v,RK} = 1386.8N$. By substituting $F_{v,RK}$ and geometric information into Equation (4), the characteristic moment capacity can be calculated as:

$$M_{RK} = F_{v,RK} \times \frac{\sum(x^2+y^2)}{r_{max}} \times n_{sp} = 2.59 \text{ kNm} \quad (5)$$

5 Application in glulam bamboo portal frames

A representable curve of the six specimens for the four types of connections was obtained by taking the average values. Fig. 10 shows the average curves of the test results, together with the analysis curve obtained from the corresponding numerical models using OpenSees. The model includes an elastic beam element, which has an identical section and material properties with the specimen, connecting with the base with a rotational spring. For the elastic beam element, modulus of elasticity and moment of inertia which related to flexural stiffness are determined by the three-point bending test of the beam specimen and beam section dimension, respectively. The modulus of elasticity is 345MPa. The initial stiffness and post-yield curve of the rotational springs are determined by subtracting the beam elastic deformation from the global response. The initial stiffness of ORL, S3FRP, S5FRP, D5FRP specimens are 31.0, 32.6, 33.0, and 37.0 kN-m, respectively. The analysis outputs fit well with the test results.

Push-over analyses were carried out on glue-laminated bamboo portal frames with various types of dowel-type connections. Both beams and columns in the portal frame have a section of 80x120mm. The member size is the same as the test specimen shown in Fig. 1. Detail of the ORL connection is applied at the column bases and beam-column connections. Three different levels of enhanced connections tested previously were also included in the analysis to evaluate the performance in real scale frame. Fig. 11 schematises the model and its dimensions. The frame model consists of an elastic beam, column elements and rotational springs. Since the dimension of the beam and column of the portal frame is the same with the

connection test specimen, these rotational springs used in the previous ORL, S3FRP, S5FRP, D5FRP models were then implemented in the portal frame model to represent semi-rigid connections.

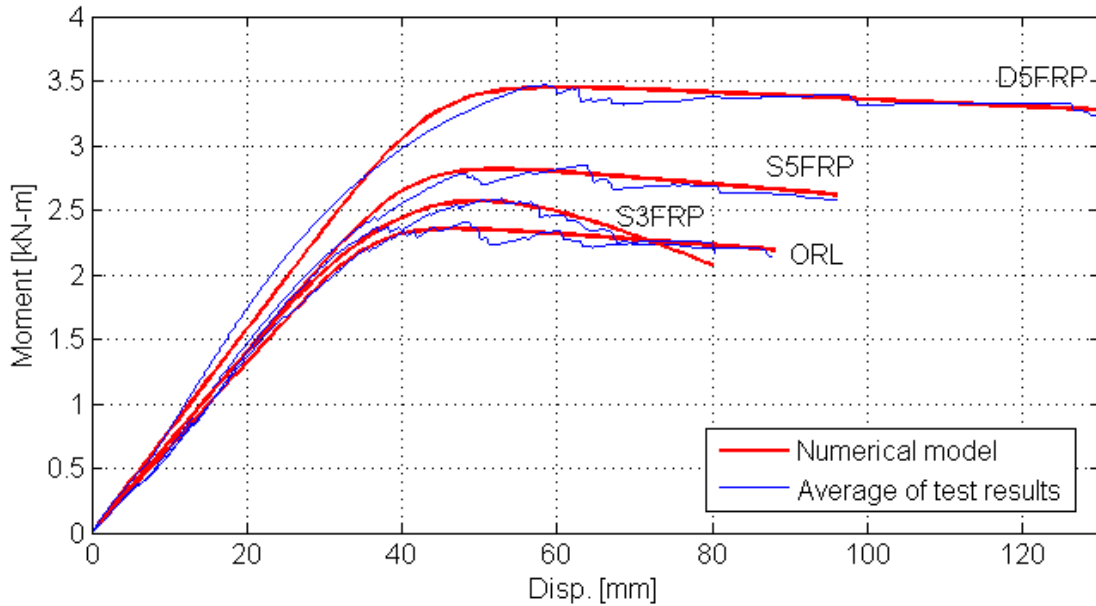


Fig. 10 Averaged load-displacement curves of specimens and the corresponding analysis curves from the numerical models

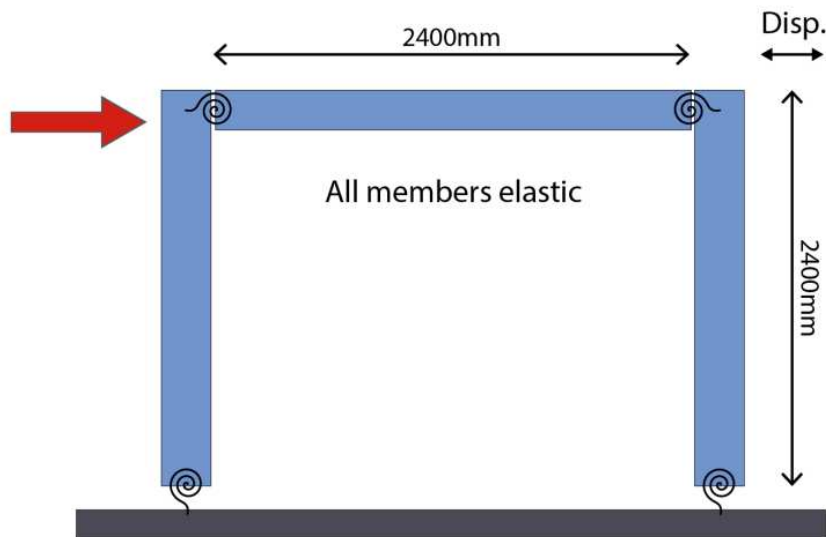


Fig. 11 Model dimensions and assumptions of the portal frame used for push-over analyses

Fig. 12 illustrates the comparison of the push-over curves of the portal frames using four different types of connections. Double-sided reinforcement connections, the D5FRP group, demonstrates significantly higher stiffness and strength. This will, for instance, benefit the robustness of the structures in the event of an earthquake. It is also noteworthy that the

glue-laminated bamboo portal frames with dowel-type connections can often undergo large displacement, of which the phenomenon was found in the case of timber portal frame (Zhang et al. 2019).

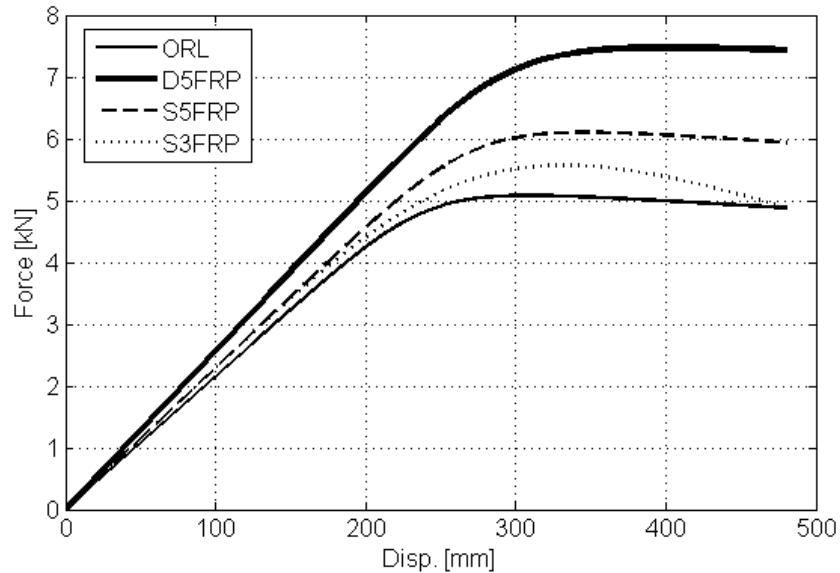


Fig. 12 Comparison of the push-over curves of the portal frames with the four different types of connections

6 Conclusion

In this paper, a series of moment connections made by Glue-Laminated Bamboo (GLB) were tested, and their reinforcement strategies were proposed. The moment-capacity and load-displacement behaviours of these connections were investigated. Further numerical analysis was carried out in a portal frame assuming the connections investigated in this study being employed to understand the impact of the reinforcement strategies proposed in this paper on the portal frame. The following conclusions could be drawn from this paper:

- (1) The dominant failure mode of the connections in all types is longitudinal splitting due to tensile stress perpendicular to the grain.
- (2) Use of single-sided GFRP reinforcement, S3FRP and S5FRP, shows improvements on both the moment capacity and the time to develop the first crack. However, the ultimate displacement may not increase due to cracks developing on the un-reinforced side of specimens.
- (3) Applying the GFRP sheet to reinforce both sides of the GLB members will significantly increase the moment capacity of 37% compared to the unreinforced group. Another benefit of this reinforcement strategy is to enable the connection to perform larger

displacement. This strategy can significantly prolong the time to develop the first crack and delay propagating the cracks in GLB connections.

- (4) Under the same rotation, corner dowels have the largest displacement and hence the most significant strain due to their largest lever arms.
- (5) Push-over analyses of a portal frame consisting of different types of connections tested in this paper confirm the advantage of double-sided reinforcement with GFRP.

Compliance with Ethical Standards

On behalf of all authors, the corresponding author states that there is no conflict of interest.

Data availability

The raw data required to reproduce these findings are available to download from [https://www.dropbox.com/sh/7tmlutgj87a90yz/AAB_ufPNS8ROOHJKtk5uxe8ga?dl=0]. The processed data required to reproduce these findings are available to download from [https://www.dropbox.com/sh/7tmlutgj87a90yz/AAB_ufPNS8ROOHJKtk5uxe8ga?dl=0]

References

- Alhayek H, Svecova D (2012) Flexural stiffness and strength of GFRP-reinforced timber beams. *J Compos Constr* 16:245–252. [https://doi.org/10.1061/\(ASCE\)CC.1943-5614.0000261](https://doi.org/10.1061/(ASCE)CC.1943-5614.0000261)
- BSI (2009) Eurocode 5 design of timber structures. British Standards Institution, London, United Kingdom
- BSI (2016) BS EN 14358: Timber structures. Calculation and verification of characteristic values. British Standards Institution, London, United Kingdom
- Chang WS (2015) Repair and reinforcement of timber columns and shear walls - A review. *Constr Build Mater* 97:14–24. <https://doi.org/10.1016/j.conbuildmat.2015.07.002>
- Chung KF, Yu WK (2002) Mechanical properties of structural bamboo for bamboo scaffoldings. *Eng Struct* 24:429–442. [https://doi.org/10.1016/S0141-0296\(01\)00110-9](https://doi.org/10.1016/S0141-0296(01)00110-9)
- De La Rosa García P, Escamilla AC, Nieves González García M (2013) Bending reinforcement of timber beams with composite carbon fiber and basalt fiber materials. *Compos Part B Eng* 55:528–536. <https://doi.org/10.1016/j.compositesb.2013.07.016>
- Gatoo A, Sharma B, Bock M, et al (2014) Sustainable structures: Bamboo standards and building codes. *Proc Inst Civ Eng Eng Sustain* 167:189–196. <https://doi.org/10.1680/ensu.14.00009>
- Gómez EP, González MN, Hosokawa K, Cobo A (2019) Experimental study of the flexural behavior of timber beams reinforced with different kinds of FRP and metallic fibers. *Compos Struct* 213:308–316. <https://doi.org/10.1016/j.compstruct.2019.01.099>

- Huang Y, Ji Y, Yu W (2019) Development of bamboo scrimber: a literature review. *J Wood Sci* 65:25. <https://doi.org/10.1186/s10086-019-1806-4>
- Kim YJ, Harries KA (2010) Modeling of timber beams strengthened with various CFRP composites. *Eng Struct* 32:3225–3234. <https://doi.org/10.1016/j.engstruct.2010.06.011>
- Lathuilière D, Bléron L, Descamps T, Bocquet JF (2015) Reinforcement of dowel type connections. *Constr Build Mater* 97:48–54. <https://doi.org/10.1016/j.conbuildmat.2015.05.088>
- Leng Y, Xu Q, Harries KA, et al (2020) Experimental study on mechanical properties of laminated bamboo beam-to-column connections. *Eng Struct* 210:110305. <https://doi.org/10.1016/j.engstruct.2020.110305>
- Li H, Wu G, Zhang Q, et al (2018) Ultimate bending capacity evaluation of laminated bamboo lumber beams. *Constr Build Mater* 160:365–375. <https://doi.org/10.1016/j.conbuildmat.2017.11.058>
- Li HT, Zhang QS, Huang DS, Deeks AJ (2013) Compressive performance of laminated bamboo. *Compos Part B Eng* 54:319–328. <https://doi.org/10.1016/j.compositesb.2013.05.035>
- Li YF, Tsai MJ, Wei TF, Wang WC (2014) A study on wood beams strengthened by FRP composite materials. *Constr Build Mater* 62:118–125. <https://doi.org/10.1016/j.conbuildmat.2014.03.036>
- Metelli G, Preti M, Giuriani E (2016) On the delamination phenomenon in the repair of timber beams with steel plates. *Constr Build Mater* 102:1018–1028. <https://doi.org/10.1016/j.conbuildmat.2015.09.038>
- Morales-Conde MJ, Rodríguez-Liñán C, Rubio-De Hita P (2015) Bending and shear reinforcements for timber beams using GFRP plates. *Constr Build Mater* 96:461–472. <https://doi.org/10.1016/j.conbuildmat.2015.07.079>
- Penellum M, Sharma B, Shah DU, et al (2018) Relationship of structure and stiffness in laminated bamboo composites. *Constr Build Mater* 165:241–246. <https://doi.org/10.1016/J.CONBUILDMAT.2017.12.166>
- Ramirez F, Correal JF, Yamin LE, et al (2012) Dowel-bearing strength behavior of glued laminated Guadua bamboo. *J Mater Civ Eng* 24:1378–1387. [https://doi.org/10.1061/\(ASCE\)MT.1943-5533.0000515](https://doi.org/10.1061/(ASCE)MT.1943-5533.0000515)
- Reynolds T, Sharma B, Harries K, Ramage M (2016) Dowelled structural connections in laminated bamboo and timber. *Compos Part B Eng* 90:232–240. <https://doi.org/10.1016/J.COMPOSITESB.2015.11.045>
- Reynolds TPS, Sharma B, Serrano E, et al (2019) Fracture of laminated bamboo and the influence of preservative treatments. *Compos Part B Eng* 174:.. <https://doi.org/10.1016/j.compositesb.2019.107017>
- Schober KU, Rautenstrauch K (2007) Post-strengthening of timber structures with CFRP's. *Mater Struct Constr* 40:27–35. <https://doi.org/10.1617/s11527-006-9128-6>
- Shah DU, Bock MCD, Mulligan H, Ramage MH (2016) Thermal conductivity of engineered bamboo composites. *J Mater Sci* 51:2991–3002. <https://doi.org/10.1007/s10853-015-9610-z>
- Shah DU, Sharma B, Ramage MH (2018) Processing bamboo for structural composites: Influence of preservative treatments on surface and interface properties. *Int J Adhes*

- Adhes 85:15–22. <https://doi.org/10.1016/J.IJADHADH.2018.05.009>
- Sharma B, Bauer H, Schickhofer G, Ramage MH (2017) Mechanical characterisation of structural laminated bamboo. *Struct Build* 170:250–264. <https://doi.org/10.1680/jstbu.16.00061>
- Sharma B, Gatóo A, Bock M, Ramage M (2015a) Engineered bamboo for structural applications. *Constr Build Mater* 81:66–73. <https://doi.org/10.1016/j.conbuildmat.2015.01.077>
- Sharma B, Gatóo A, Ramage MH (2015b) Effect of processing methods on the mechanical properties of engineered bamboo. *Constr Build Mater* 83:95–101. <https://doi.org/10.1016/j.conbuildmat.2015.02.048>
- Sharma B, Shah DU, Beaugrand J, et al (2018) Chemical composition of processed bamboo for structural applications. *Cellulose* 25:3255–3266. <https://doi.org/10.1007/s10570-018-1789-0>
- Shekarchi M, Vatani Oskouei A, Raftery GM (2020) Flexural behavior of timber beams strengthened with pultruded glass fiber reinforced polymer profiles. *Compos Struct* 241:112062. <https://doi.org/10.1016/j.compstruct.2020.112062>
- Tang G, Yin L, Li Z, et al (2019) Structural behaviors of bolted connections using laminated bamboo and steel plates. *Structures* 20:324–339. <https://doi.org/10.1016/j.istruc.2019.04.001>
- Titirla M, Michel L, Ferrier E (2019) Mechanical behaviour of glued-in rods (carbon and glass fibre-reinforced polymers) for timber structures—An analytical and experimental study. *Compos Struct* 208:70–77. <https://doi.org/10.1016/j.compstruct.2018.09.101>
- Triantafillou TC (1997) Shear Reinforcement of Wood Using FRP Materials. *J Mater Civ Eng* 9:65–69
- Trujillo D, Ramage M, Chang W-S (2013) Lightly modified bamboo for structural applications. *Proc Inst Civ Eng Constr Mater* 166:238–247. <https://doi.org/10.1680/coma.12.00038>
- Trujillo OE, Wang T-H (2015) Parametric modeling of bamboo pole joints
- Wang TH, Espinosa Trujillo O, Chang WS, Deng B (2017) Encoding bamboo's nature for freeform structure design. *Int J Archit Comput* 15:169–182. <https://doi.org/10.1177/1478077117714943>
- Yang Y, Liu J, Xiong G (2013) Flexural behavior of wood beams strengthened with HFRP. *Constr Build Mater* 43:118–124. <https://doi.org/10.1016/j.conbuildmat.2013.01.029>
- Zhang C, Guo H, Jung K, et al (2019) Using self-tapping screw to reinforce dowel-type connection in a timber portal frame. *Eng Struct* 178:656–664. <https://doi.org/10.1016/j.engstruct.2018.10.066>
- Zhou J, Huang D, Ni C, et al (2018) Experiment on Behavior of a New Connector Used in Bamboo (Timber) Frame Structure under Cyclic Loading. *Adv Mater Sci Eng* 2018:. <https://doi.org/10.1155/2018/9084279>